RSC Advances

PAPER

View Article Online
View Journal | View Issue

Open Access Article. Published on 10 September 2024. Downloaded on 1/15/2026 11:51:11 AM.
This article is licensed under a Creative Commons Attribution-NonCommercial 3.0 Unported Licence.

Check for updates

Cite this: *RSC Adv.*, 2024, **14**, 28669

Design, synthesis, analgesic, antibacterial and docking studies of novel 8-piperazinylcaffeine carboxylate ionic liquids†

Mohammad Navid Soltani Rad, *[ab] Somayeh Behrouz, *[ab] Parichehr Halaj Yazdi,[a] Seyedeh-Sara Hashemi [c] and Marzieh Behrouz [a]

This paper presents a comprehensive evaluation of novel 8-piperazinylcaffeine carboxylate ionic liquids, including their design, synthesis, characterization, analgesic and antibacterial properties, as well as docking studies. These unique salts were produced by combining 8-piperazinyl caffeine (**8-PC**) with various carboxylic acids, some of which are commonly used nonsteroidal anti-inflammatory drugs (NSAIDs). Through *in vivo* experiments on female mice using the formalin test, the analgesic efficacy of different **8-PC** salts with various NSAIDs was assessed. Results demonstrated that a majority of these salts exhibited significant analgesic activity when compared to NaIBP, a standard reference drug. Particularly noteworthy was the enhanced analgesic effect of the **8-PC**'s NSAIDs salts (**11a**, **11c–e**, and **11k**) compared to their corresponding sodium salts, which was attributed to the presence of the **8-PC** cation (synergistic effect). Furthermore, all synthesized salts were subjected to *in vitro* testing against Gram-positive *Staphylococcus aureus* (PTCC 1133), Gram-negative *Pseudomonas aeruginosa* (ATCC 27853), and *Escherichia coli* (PTCC 1330) bacteria. Among them, salt **11k** displayed notable antibacterial activity, especially against *P. aeruginosa*, a dangerous opportunistic pathogen. Additionally, docking analysis revealed strong binding of the synthesized **8-PC** and NSAID salts to the active site of the COX-2 enzyme.

Received 29th August 2024
Accepted 4th September 2024

DOI: 10.1039/d4ra06244b

rsc.li/rsc-advances

1 Introduction

Undoubtedly, one of the most important discoveries in the chemistry era that happened at the end of the 20th century is the synthesis and application of ionic liquids.[1] Ionic liquids have garnered a lot of attention in the last ten years because of their tunable and environmentally friendly physicochemical characteristics.[2] Ionic liquids are now categorized into three groups based on their applications due to the field's ongoing development.[3] Paul Walden discovered the first-generation ILs in 1914, and they have certain physical characteristics like low melting point, low vapor pressure and, good thermal stability.[4] The majority of first-generation ionic liquids are not very biodegradable, according to additional research.[5] Second-generation ILs are being developed for lubricants, metal ion complexing agents, and energy-related functional materials.[6] The third generation of ionic liquids involves the development of task-specific or functionalized ionic liquids in particular active pharmaceutical ingredients ionic liquids (APIs-ILs).[7] The first and second generations of ILs have been the subject of a great deal of research; however, in recent years, the third generation of ILs has demonstrated significant promise for biological action, including antibacterial, anticholinergic, antifungal, deterrent, and so on.[8] Designing the APIs-ILs is a critical step in drug development. In this respect, the conversion of a drug into its corresponding API-IL is greatly fabulous since the pharmacokinetics of a drug candidate, particularly the absorption or membrane-transfer process, can be greatly impacted by the choice of salt ion.[9] Consequently, there may be a variation or modulation in the time course of its pharmacodynamic and toxicological effects. This can be highly helpful to formulators and chemists in many areas of drug research and discovery.[9]

In general, the API-ILs can be classified into four categories. The classification of API-ILs is shown in Fig. 1. Among the API-ILs types, the API-ILs comprising two APIs are interesting since the counter-ion can be chosen and tuned to synergistically enhance the desired effects or to neutralize unwanted side effects of the active entity. They involve similar biological active ion-pairs (SBAIP) and dissimilar biological active ion-pairs (DSBAIP). The counter-ion in DSBAIP can also be chosen to

[a]*Department of Chemistry, Shiraz University of Technology, Shiraz 71555-313, Iran. E-mail: soltani@sutech.ac.ir; behrouz@sutech.ac.ir; Fax: +98 71 3735 4520; Tel: +98 71 3735 4500*

[b]*Medicinal Chemistry Research Laboratory, Novel Technology for Health Research Center, Shiraz University of Technology, Shiraz 71555-313, Iran*

[c]*Burn and Wound Healing Research Center, Division of Food and Nutrition, Shiraz University of Medical Sciences, Shiraz, Iran*

† Electronic supplementary information (ESI) available. See DOI: https://doi.org/10.1039/d4ra06244b

© 2024 The Author(s). Published by the Royal Society of Chemistry

Open Access Article. Published on 10 September 2024. Downloaded on 1/15/2026 11:51:11 AM.
This article is licensed under a Creative Commons Attribution-NonCommercial 3.0 Unported Licence.

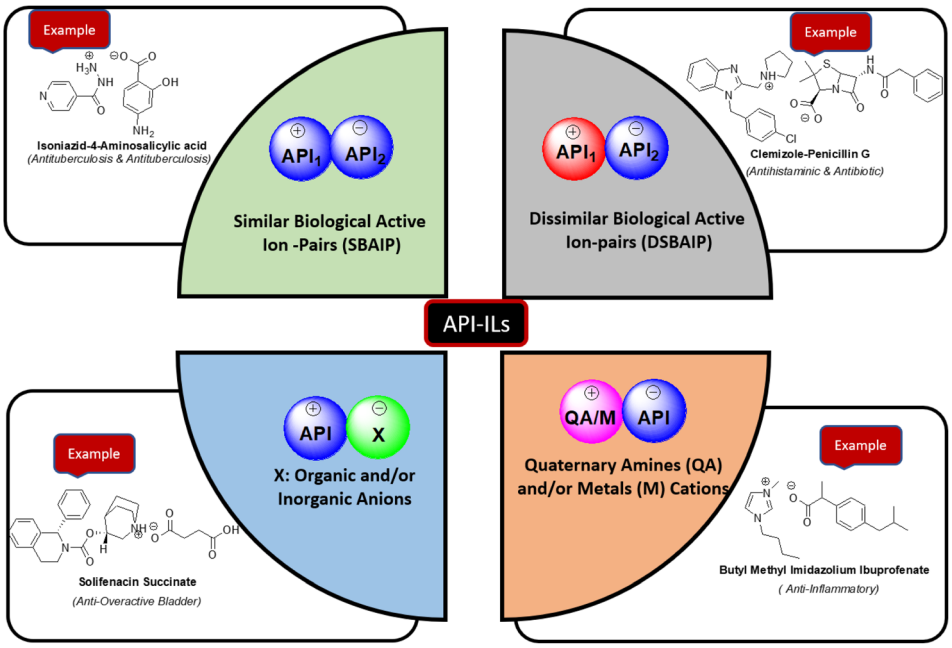

Fig. 1 The classification of API-ILs types with their corresponding examples.[8,11]

pharmacologically act independently, but therapeutically in a synergistic manner.[10,11]

The C8-modified caffeine derivatives have immense pharmaceutical properties.[12,13] We recently discussed and classified C8-modified caffeine derivatives into C8–C, C8–O, C8–S, and C8–N based on the type of atom linked to C8.[14] Among these derivatives, the C8–N analogues are particularly noteworthy for their significant biological activities, including anticancer, antimicrobial, antiviral, and CNS stimulant properties.[14] Fig. 2 illustrates the structures of certain C8–N derivatives **1–10** and their respective biological activities.

Piperazine is a significant molecule in medicinal chemistry due to its diverse pharmacological properties.[15] It is a heterocyclic organic compound that contains two nitrogen atoms in a six-membered ring, which makes it an important building block for designing drugs.[16] This heterocyclic compound has a high affinity for binding to enzyme or receptor active sites due to the presence of two lone pairs oriented in opposite directions.[17] Piperazine derivatives have been found to exhibit a wide range of biological activities such as antipsychotic, antihistaminic, anti-inflammatory, antiviral, and anticancer effects.[18] Moreover, piperazine has been utilized as a scaffold for developing drugs that target various diseases, including schizophrenia, anxiety disorders, depression, and cancer. Due to its versatile nature, piperazine has become an essential component in the field of medicinal chemistry, and its derivatives continue to be investigated for their therapeutic potential.[19]

The linking of the piperazine moiety to the caffeinyl core in caffeine C8–N derivatives is intriguing, particularly in light of previous indications that coupling piperazinyl and/or 1,4-diazepanyl cores to the C8 position of certain xanthines resulted in a variety of biological effects, such as antidiabetic mellitus type I and type II, anti-arthritis, anti-obesity, inhibition of allograft transplantation, and osteoporosis inhibition caused by calcitonin [20]. The 8-piperazinyl caffeine (**8-PC**) is a useful compound due to its exceptional properties like water solubility, remarkable basic character (pH ≈ 12.5 in 0.01 M aqueous solution at 25 °C) and nucleophilic nature that can be extensively utilized in the synthesis of new drug candidates. Recently, we reported 8-(4-alkylpiperazinyl) caffeine (**9**) and 8-piperazinyl caffeinyl-triazolylmethyl hybrid conjugates (**10**) exhibiting remarkable leishmanicidal and anticancer properties, respectively.[21,22]

Pain relievers hold significant importance in the realm of healthcare and wellness. These medications play a crucial role in alleviating discomfort, reducing inflammation, and managing chronic conditions. Whether it be a headache, muscle soreness, or a more severe issue such as arthritis, pain relievers provide relief and improve quality of life for countless individuals.[23]

Nonsteroidal anti-inflammatory drugs (NSAIDs) are a class of medications commonly used to reduce pain, inflammation, and fever.[24] While NSAIDs offer effective relief for many people, they are associated with several potential problems and risks. Several important concerns with NSAIDs comprise stomach irritation, ulcers, and bleeding in the digestive tract the kidney damage, heart attack, stroke, and other cardiovascular events is happened when NSAIDs are taken in high doses.[25] One reason for the risk associated with using high doses of NSAIDs may be attributed to the drugs' poor pharmacokinetics, particularly their lack of solubility.[26] Therefore, converting NSAIDs to their corresponding ILs can help to address these shortcomings.

Owing to the exceptional biological activity of 8-caffeinyl derivatives and also the promising pharmaceutical profiles of **8-PC** analogues in rational drug design for promoting drugs' potencies, hereby we would like to report the synthesis, characterization, analgesic, antibacterial and *in silico* assessment of new 8-piperazinylcaffeine carboxylate ionic liquids (**11**). The

 © 2024 The Author(s). Published by the Royal Society of Chemistry

Open Access Article. Published on 10 September 2024. Downloaded on 1/15/2026 11:51:11 AM.
This article is licensed under a Creative Commons Attribution-NonCommercial 3.0 Unported Licence.

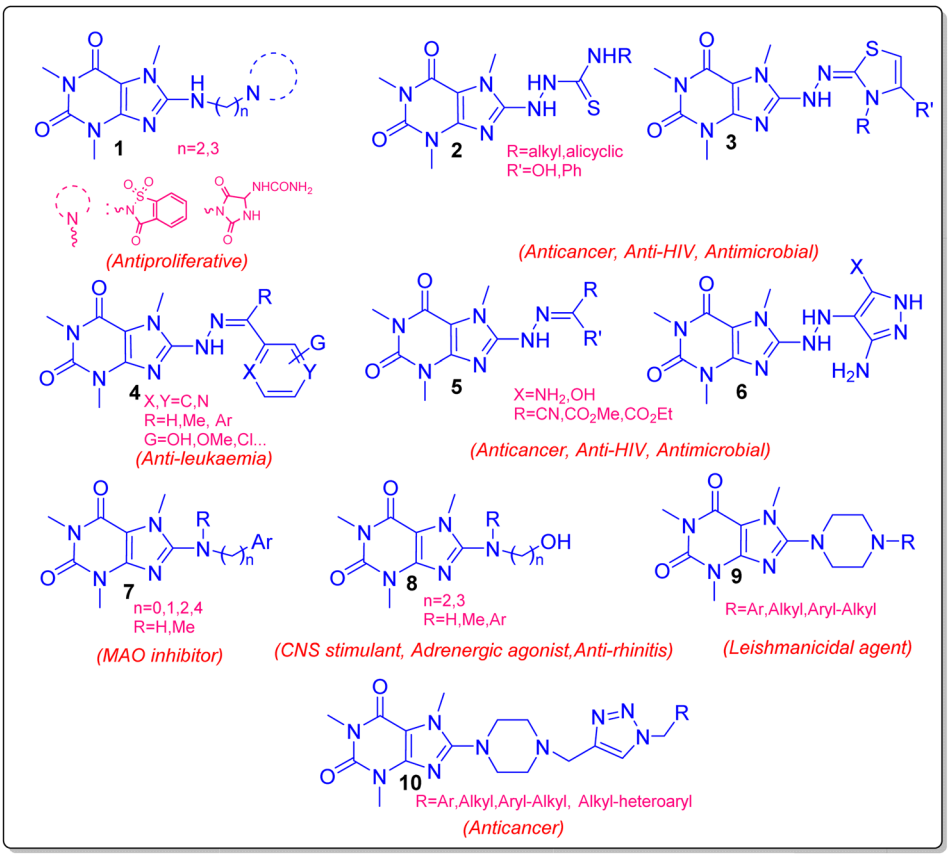

Fig. 2 The structure of some C8–N caffeine derivatives and their related biological activity.[14]

general structure of these new API-ILs is shown in Fig. 3. As shown in Fig. 3, the title compounds are carboxylate salts of 8-piperazinylcaffeine in which some carboxylates are NSAIDs or bioactive carboxylates.

2 Results and discussion

2.1. Chemistry

The general synthetic pathway for the synthesis of title salts **11** is illustrated in Scheme 1.

The synthesis was started by preparing 8-bromocaffeine (**8-BC**). The aim was to brominate caffeine in order to increase the positive charge density on C(8) for the subsequent S_NAr-type reaction. The standard procedure for synthesizing **8-BC** involved using NBS in a mixture of DCM and water at room temperature.[27] While other methods also exist for synthesizing **8-BC**,[28,29] none were as effective as using NBS. The NBS method resulted in almost pure **8-BC** in a quantitative yield (>99%). After obtaining **8-BC**, 8-piperazinyl caffeine (**8-PC**) was produced through a S_NAr-type coupling reaction of piperazine with the electrophilic C(8) of **8-BC** in DMF at 100 °C.[21] As previously mentioned, **8-PC**, due to the presence of a piperazinyl moiety, exhibits remarkable basic properties. Among the nitrogens present in the piperazinyl moiety of **8-PC**, the N-atom linked to C(8) is a weak base because of the electron-withdrawing nature of the caffeinyl residue. However, despite this, the N(4)-atom demonstrates strong basic behavior, enabling it to react with various organic acids and form the corresponding salts. To achieve this, **8-PC** was dissolved in anhydrous DCM or $CHCl_3$, and the desired acid was then added and stirred at room temperature to obtain the corresponding salts, whose structures are illustrated in Fig. 4.

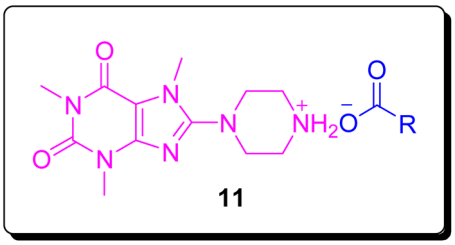

Fig. 3 The general structure of 8-piperazinylcaffeine carboxylate ionic liquids (**11**).

As shown in Fig. 4, various carboxylic acids can be utilized to produce their respective salts. Specifically, drugs containing a carboxyl group can be employed to generate salts with **8-PC**. For example, a variety of NSAIDs such as aspirin, mefenamic acid, ibuprofen, naproxen, and salicylic acid were used to synthesize the corresponding salts **11a**, **11c–e**, and **11k** with good to excellent yields, respectively. Additionally, other aliphatic or aromatic carboxylic acids yielded salts with **8-PC** in good to excellent yields as well.

Open Access Article. Published on 10 September 2024. Downloaded on 1/15/2026 11:51:11 AM.
This article is licensed under a Creative Commons Attribution-NonCommercial 3.0 Unported Licence.

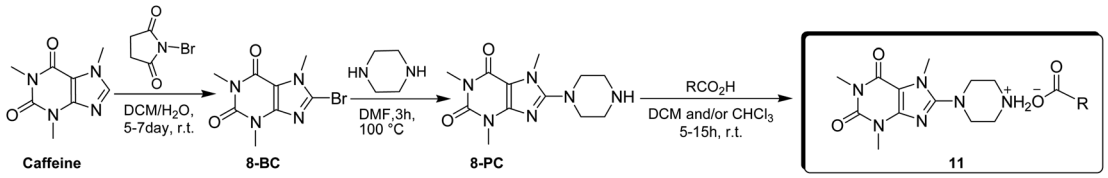

Scheme 1 General synthetic pathway for preparing novel 8-piperazinylcaffeine carboxylate ionic liquids **11**.

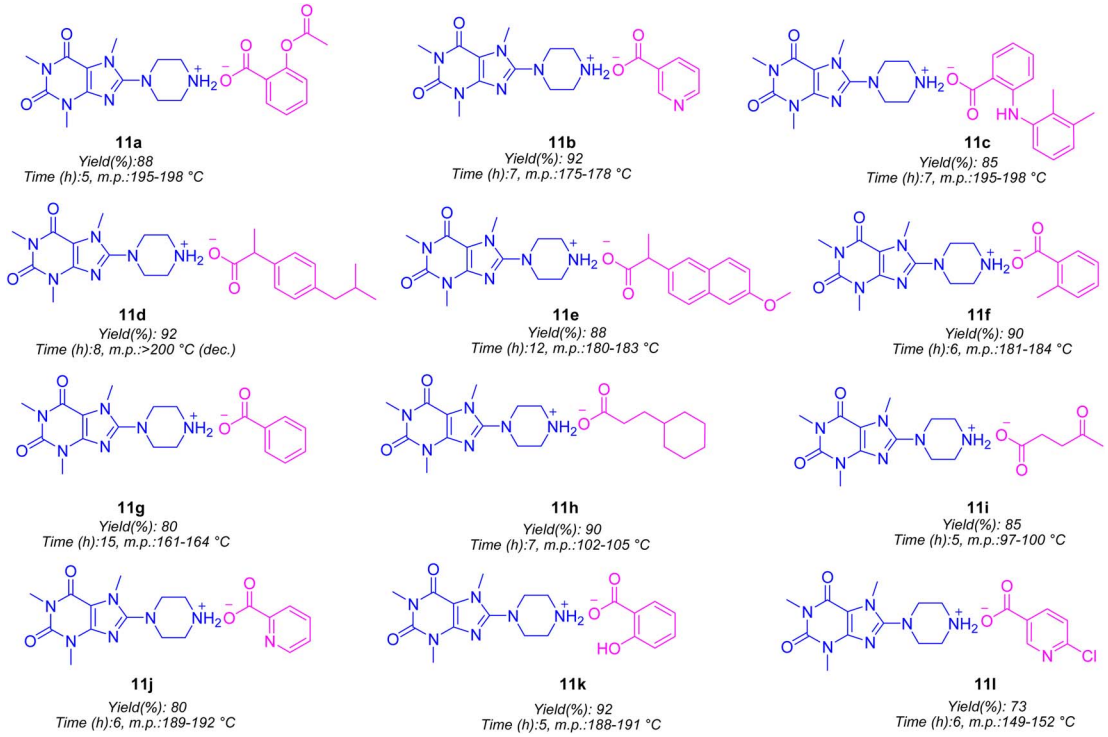

Fig. 4 The structures of 8-piperazinylcaffeine carboxylate ionic liquids **11a–11l**.

2.2. The biological assessment

2.2.1. Formalin test. The formalin test is a widely used chemical assessment method for inflammatory pain caused by injuries. It is considered a more reliable representation of clinical pain and serves as an effective tool for evaluating new compounds, as it covers various mechanisms of pain perception including inflammation, nerve-related pain, and central processes. One key benefit of the formalin test compared to other inflammatory pain models is that by injecting a diluted formalin solution into the hindpaw of a mouse or rat, it can simulate both immediate and prolonged pain responses using a single chemical within a relatively short timeframe.[30] In this research, the reaction of animals to pain induced by formalin was evaluated.

The pain-relieving impact curves of the synthetic compound ibuprofen (NaIBP), as well as the control and blank groups, were graphed. Fig. 5A–D illustrates the pain scores over time for synthetic compounds **11a**, **11c–e**, and **11k**, respectively. In Fig. 5, it is evident that synthetic compounds **11a**, **11c–e**, and **11k** exhibit superior analgesic properties compared to NaIBP, the blank group, and the control, in particular within the initial 5 minutes of oral administration. Compound **11c** (Fig. 5B) demonstrated particularly potent activity, with a pain score of 0.63 at 5 minutes, surpassing NaIBP and others. Following closely behind, compound **11k** (Fig. 5E) exhibited slightly lower pain relief at 5 minutes (0.65) but even stronger than **11c** at 10 minutes. Compound **11k** almost is weaker than **11c** in effectiveness at subsequent time intervals. When compound **11a** (Fig. 5A) was administered, the animals experienced pain relief within 5 minutes, demonstrating a stronger analgesic effect compared to NaIBP across various time intervals. Compound **11e** (Fig. 5D) exhibited either stronger or nearly equal activity compared to NaIBP at different time points. Compound **11d** (Fig. 5C), which also contains the ibuprofenate anion, demonstrated increased efficacy over NaIBP, particularly between 10–20 minutes; however, its effectiveness decreased at 25 minutes in comparison to NaIBP.

As previously discussed, salt **11d** demonstrates enhanced activity compared to NaIBP, despite both compounds sharing a common ibuprofenate structure. This raises important questions about the factors contributing to the increased analgesic

 © 2024 The Author(s). Published by the Royal Society of Chemistry

Open Access Article. Published on 10 September 2024. Downloaded on 1/15/2026 11:51:11 AM.
This article is licensed under a Creative Commons Attribution-NonCommercial 3.0 Unported Licence.

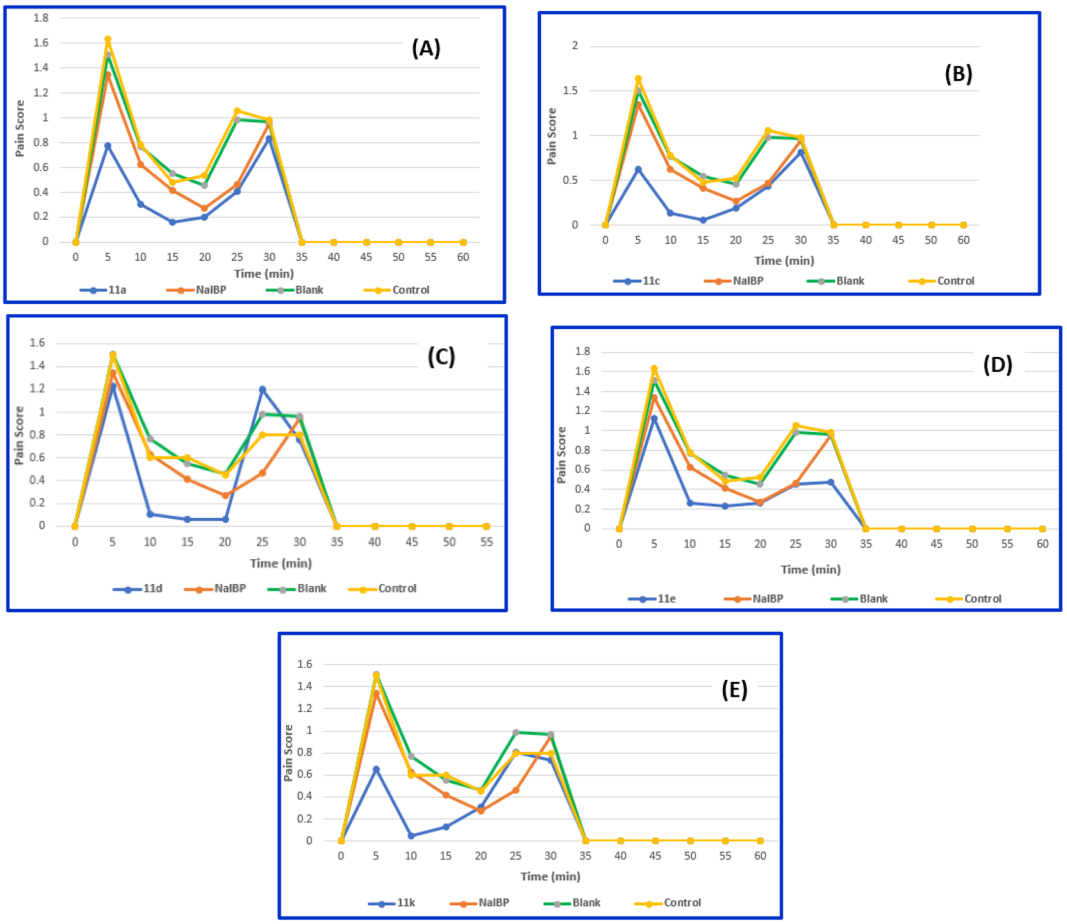

Fig. 5 Analgesic effect curves (A–E) of the synthetic compounds **11a**, **11c–e**, and **11k**.

efficacy of **11d** relative to NaIBP. Additionally, does this trend hold true for other salts when compared to their sodium counterparts? What role does **8-PC** play in this context? Does it possess its own analgesic properties that could mimic the effects of the corresponding salts?

To address these questions, we investigated and compared the analgesic profiles of salts **11a**, **11c–e**, and **11k** with their respective sodium salts, as well as with the hydrochloride salt of **8-PC** (**8-PC**·HCl). Although **8-PC** is sufficiently soluble in distilled water, we opted to convert it to **8-PC**·HCl prior to testing to ensure consistent ionic conditions across all samples. The results are presented in Fig. 6.

As indicated by the pain-relieving impact curves (A–B), the **8-PC** salt (**8-PC**·HCl) shows no significant analgesic activity compared to the other synthesized salts tested, particularly at the 5–15 minutes mark. However, **8-PC**·HCl does provide slight pain relief, primarily observed at the 20-minutes measurement. Notably, **8-PC**·HCl exhibits analgesic activity similar to that of sodium aspirinate (NaASP), sodium ibuprofenate (NaIBP), and sodium naproxenate (NaNAP). Additionally, at the 20-minutes mark, **8-PC**·HCl demonstrates comparable analgesic effects to compounds **11e** and **11k**.

We also assessed the effects of sodium salts of the NSAIDs used in this study and compared them with the synthesized compounds. As shown in curves A–B (Fig. 6), the sodium salts of the NSAIDs demonstrated weaker analgesic activity compared to their corresponding synthesized salts, particularly at the 5–10 minutes interval, which is critical for acute pain relief. In curve F, while NaASP exhibited slightly lower analgesic activity at 5 minutes, it showed diminished activity at other time points, except at 25 minutes. Compounds **11c** and **11k** displayed significant differences in analgesic activity compared to their related sodium salts. For **11d**, a substantial difference in activity was observed, especially at the 10–20 minutes interval, whereas **11e** showed nearly equivalent activity during the same period.

Based on the findings, it can be deduced that the **8-PC** counterion present in the salts under investigation plays a pivotal role in amplifying the analgesic efficacy of the sodium salts of NSAIDs, indicating a synergistic effect. This observation aligns with existing literature that suggests certain compounds or medications have the potential to augment the analgesic properties of NSAIDs.[31–33] Notably, combinations of caffeine with widely recognized NSAIDs like ibuprofen, aspirin, and acetaminophen are extensively utilized in contemporary medicine. It is well-documented that caffeine notably enhances the analgesic effects of NSAIDs.[34–39]

2.2.2. Toxicity studies. The animals were monitored for a month following the administration of the synthesized

Open Access Article. Published on 10 September 2024. Downloaded on 1/15/2026 11:51:11 AM.
This article is licensed under a Creative Commons Attribution-NonCommercial 3.0 Unported Licence.

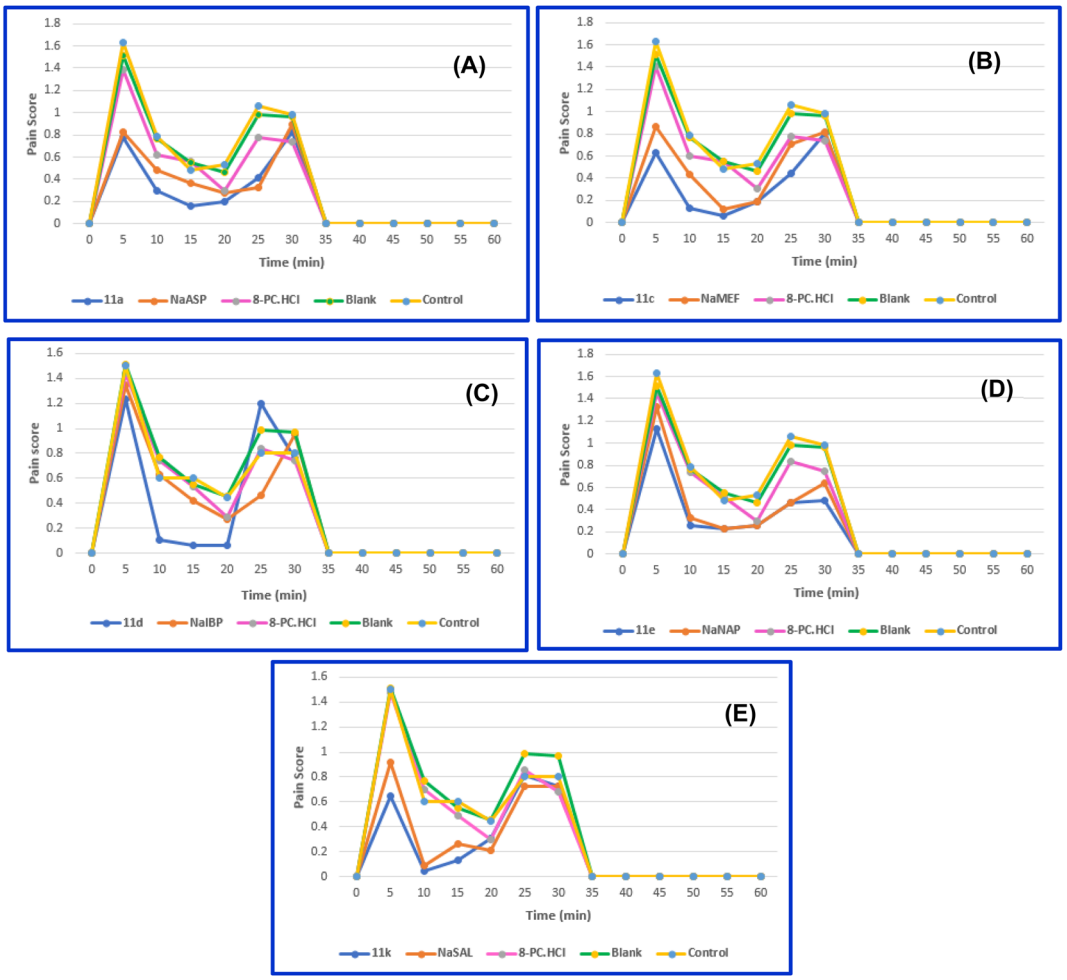

Fig. 6 Analgesic effect curves (A–E) of salts **11a**, **11c–e**, and **11k**.

compounds **11a**, **11c–e**, and **11k**, and the mortality rate was documented. It was noted that there were no instances of mortality attributed to the toxicity of the synthesized compounds.

2.2.3. Antibacterial screening tests. The antibacterial profile of title compounds **11a–11l** was *in vitro* assessed in diverse concentrations of 0.0062, 0.0125, 0.025 and 0.05 mg mL^{-1} against *Staphylococcus aureus* (PTCC 1133) as a Gram-positive bacterium, *Pseudomonas aeruginosa* (ATCC 27853), and *Escherichia coli* (PTCC 1330) as Gram-negative bacteria. Ethacridine lactate (Acrinol) was used as a reference drug. The acrinol was selected as a reference drug since it has ionic structure and can be ionized like title compounds. The "+" or "−" notation is commonly used to show the presence or absence of antibacterial activity. The "+" notation represented the antibacterial activity or prevention of bacterial growth and "−" notation represented that entry does not have antibacterial behavior or unable to stop bacterial growth. The results are depicted in Table 1.

As indicated in Table 1, compound **11a** shows no impact on the tested bacteria. Conversely, compounds **11b**, **11i**, and **11j** inhibit the growth of *S. aureus* and *P. aeruginosa* at a concentration of 0.05 mg mL^{-1}. Moreover, compounds **11c**, **11d**, **11h**, and **11l** affect bacterial growth at varying concentrations of 0.0125, 0.025, and 0.05 mg mL^{-1}. Compounds **11e** and **11g** salts are effective against *E. coli* at concentrations of 0.025 and/or 0.05 mg mL^{-1}, while compound **11f** demonstrates activity against both tested Gram-negative bacteria. Notably, the salt of compound **11k** containing the salicylate anion exhibits the highest potency against all tested bacteria across all concentrations. In contrast to acrinol, this salt is particularly effective against *P. aeruginosa*, a notorious resistant and opportunist bacterium responsible for hospital-acquired infections in immunocompromised individuals such as those with neutropenia, burn injuries, and cystic fibrosis.[40] Thus, salt **11k** can be considered as an agent for fighting against both Gram-positive and Gram-negative pathogenic bacteria.

As previously discussed, salt **11k** emerged as the most effective compound against all tested bacterial strains. This raises an important question: which component of **11k** is responsible for its notable antibacterial properties? To investigate this, we conducted *in vitro* antibacterial screenings of **8-PC**·HCl and sodium salicylate against the bacteria under study. The results, presented in Table 1, suggest that the antibacterial efficacy of salt **11k** primarily stems from the salicylate anion, known for its specific antibacterial properties.[41,42] Additionally,

 © 2024 The Author(s). Published by the Royal Society of Chemistry

Open Access Article. Published on 10 September 2024. Downloaded on 1/15/2026 11:51:11 AM. This article is licensed under a Creative Commons Attribution-NonCommercial 3.0 Unported Licence.

Table 1 The *in vitro* antibacterial assessment of synthesized salts against some pathogenic bacteria

	Antibacterial screening											
	S. aureus				*P. aeruginosa*				*E. coli*			
Compound	0.0062[a]	0.0125	0.025	0.05	0.0062	0.0125	0.025	0.05	0.0062	0.0125	0.025	0.05
11a	–	–	–	–	–	–	–	–	–	–	–	–
11b	–	–	–	+	–	–	–	+	–	–	–	–
11c	–	–	+	+	–	–	–	+	–	–	+	+
11d	–	–	–	+	–	–	–	+	–	+	+	+
11e	–	–	–	–	–	–	–	–	–	–	+	+
11f	–	–	–	–	–	–	–	+	–	–	+	+
11g	–	–	–	–	–	–	–	–	–	–	–	+
11h	–	–	–	+	–	–	–	+	–	–	–	+
11i	–	–	–	+	–	–	–	+	–	–	–	–
11j	–	–	–	+	–	–	–	+	–	–	–	–
11k	+	+	+	+	+	+	+	+	+	+	+	+
11l	–	–	–	+	–	–	–	+	–	–	+	+
8-PC·HCl[b]	–	–	+	+	–	–	–	–	–	–	–	+
NaSAL[c]	–	+	+	+	–	–	–	+	+	+	+	+
Acrinol[d]	+	+	+	+	–	–	–	–	+	+	+	+

[a] Concentration (mg mL^{-1}). [b] 8-Piperazinyl caffeine hydrochloride. [c] Sodium salicylate. [d] Acrinol: ethacridine lactate.

the antibacterial activity of **8-PC**·HCl was limited, showing effectiveness only at concentrations of 0.025 and 0.05 mg mL^{-1} against *Staphylococcus aureus* and 0.05 mg mL^{-1} against *Escherichia coli*. These findings indicate that, much like its analgesic effects, **8-PC**·HCl likely serves a synergistic role in enhancing the antibiotic potency of salicylic acid.

2.3. Molecular docking study

Molecular docking studies are a widely-used and effective method for analyzing potential interactions between drug candidates and the binding sites of target receptors or enzymes. To explore the binding mode and interactions of synthesized ILs with strong analgesic properties, a molecular docking study was conducted on the active site of the target enzyme. Specifically, the docking analysis of ILs **11a**, **11c**, **11d**, **11e**, and **11k**, identified as the most potent compounds, was carried out using Molegro Virtual Docker (MVD 6.0) software with default settings.[43] Previous studies have indicated that the anti-inflammatory and analgesic effects of IBP result from the inhibition of the COX-2 enzyme.[44] Consequently, the crystal structure of murine cyclooxygenase-2 (COX-2) complexed with IBP (PDB code: 4PH9) was selected as a reference template. The ligand-bound crystallographic structure of COX-2 (4PH9) with a resolution of 1.81 Å was retrieved from the Protein Data Bank (**http://www.rcsb.org**). The enzyme structure was modified by assigning hydrogen positions based on default rules, compensating for any missing hydrogens, and removing water molecules, non-binding ligands, and introducing new ligands. Following adjustments to the enzyme structure, correct atom and bond types were defined. Subsequently, a docking study consisting of 50 independent runs was conducted to analyze the binding poses of the selected compounds with the COX-2 enzyme. The active site of the COX-2 enzyme was delineated by amino acid residues within a 7 Å radius surrounding IBP, acetyl salicylate, mefenamate, ibuprofenate, naproxenate, and salicylate anions, as well as the **8-PC** cation. Geometry optimization of the selected compounds and IBP was carried out using the PM6 method with the Gaussian09 program package.[45,46] The docking setup validation was conducted by re-docking the co-crystallized IBP at the active site of COX-2. Previous studies have suggested that an RMSD value of less than 2 Å is sufficient to confirm the accuracy of the docking setup.[47] In this study, the RMSD value between the docked and co-crystallized IBP was found to be 1.15 Å, confirming the reliability of the docking protocol. Subsequently, this validated protocol was utilized to explore the interaction and binding modes of ILs **11a**, **11c**, **11d**, **11e**, and **11k** with the active site of the COX-2 enzyme. A comparison of the docked conformations of acetyl salicylate, mefenamate, ibuprofenate, naproxenate, and salicylate anions, along with the **8-PC** cation and IBP, at the binding site of the COX-2 enzyme is depicted in Fig. 7 (on the left). Interestingly, similar to IBP, acetyl salicylate, mefenamate, ibuprofenate, naproxenate, and salicylate anions were all observed at the same binding site. However, the **8-PC** cation was situated outside the active site and interacted with amino acids in close proximity to the active site. All synthesized compounds were stabilized in the active site of the COX-2 enzyme through various interactions, including hydrogen bonding, van der Waals forces, hydrophobic interactions, and electrostatic interactions.

IBP was found to be situated near the apex of the COX-2 active site during its binding to the COX-2 enzyme.[48] Among the various amino acids near the entrance of the COX-2 enzyme's active site, Arg121 and Tyr356 are vital for facilitating the interaction between the enzyme and IBP.[49] The guanidinium moiety of Arg121 and the hydroxyl group of Tyr356 are involved in forming hydrogen bonds with the carboxylate group of IBP. No electrostatic interaction was observed between IBP and the target

Open Access Article. Published on 10 September 2024. Downloaded on 1/15/2026 11:51:11 AM.
This article is licensed under a Creative Commons Attribution-NonCommercial 3.0 Unported Licence.

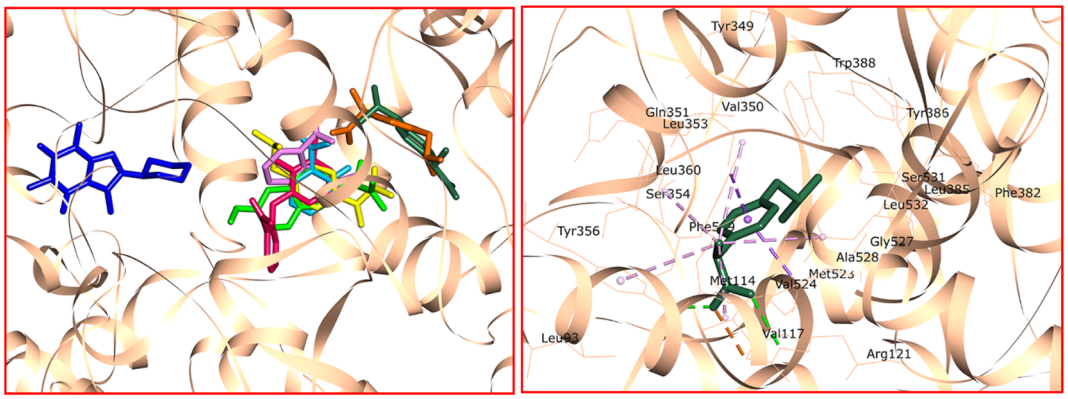

Fig. 7 Overlay view of docked conformations of acetyl salicylate (violet), mefenamate (magenta), ibuprofenate (yellow), naproxenate (green), and salicylate (cyan) anions as well as **8-PC** cation (blue), re-docked IBP (dark green), and co-crystallized IBP (orange) (left); docked conformation and interactions of re-docked IBP (right) in the active site of COX-2 enzyme.

enzyme. Additionally, hydrophobic interactions between the lipophilic portions of IBP and the amino acids present in the substrate channel help stabilize IBP in the enzyme's active site. Val350 and Ala528 contribute to π–σ interactions with the benzyl moiety of IBP. Moreover, Val350, Leu353, Val524, and Ala528 engage in van der Waals and hydrophobic interactions with the benzyl moiety of IBP. Val117, Val350, Leu532, and Leu360 participate in hydrophobic interactions with α-Me group of IBP, while Tyr356 is involved in a π–alkyl interaction with the same group. Furthermore, several hydrophobic interactions were identified between the isobutyl moiety of IBP and Leu353, Leu385, Trp388, Phe519, Met523, Val524, Leu526, Gly527, Ala528, and Ser531. The guanidinium residue of Arg121 forms a salt bridge with the carboxyl group of IBP. The docked conformation and interactions of IBP within the active site of the COX-2 enzyme are illustrated in Fig. 7 (right).

The **8-PC** cation was situated outside of the active site cavity, engaging in van der Waals, carbon–hydrogen bond, and electrostatic interactions as depicted in Fig. 8 (left). The piperazine and caffeine components of the **8-PC** cation formed carbon–hydrogen bond interactions with Gln371 and Phe372, respectively. van der Waals interactions were observed between the **8-PC** cation and Thr119, Ser122, Leu124, Leu125, Asp126, Ser127, Gln371, Phe372, and Gln373. Additionally, the oxygen and nitrogen atoms of the **8-PC** cation participated in electrostatic interactions with adjacent amino acids near the active site.

The docked conformation of the acetyl salicylate anion in the active site of the COX-2 enzyme is depicted in Fig. 8 (right). Both carboxylate moieties engaged in three robust hydrogen bonds with Arg121 and Tyr356. The phenyl ring of the acetyl salicylate anion interacted with Val89 and Val117 through two π–alkyl interactions. Furthermore, a π–cation interaction was observed between Arg121 and the phenyl ring of the ligand. Electrostatic interactions between acetyl salicylate and the target enzyme were also identified. Additionally, the acetyl salicylate anion was stabilized in the active site through van der Waals interactions involving Thr85, Pro86, His90, Leu93, Tyr116, Val117, Ser120, Phe358, Leu360, Val524, Ala528, and Leu532.

Likewise, the docked conformation and interactions of the mefenamate anion in the active site of the COX-2 enzyme are illustrated in Fig. 9 (left). The mefenamate anion was anchored in the active site of the target enzyme through electrostatic interactions, a single strong conventional hydrogen bond between Arg121 and the carboxylate group of the mefenamate anion, as well as several carbon–hydrogen bond interactions with the enzyme's active site. The π–σ and two π–alkyl interactions were

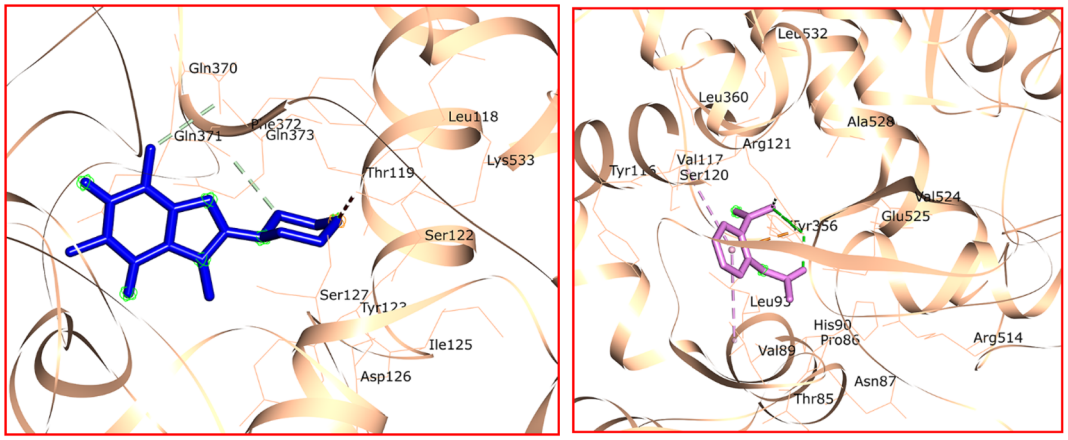

Fig. 8 Docked conformations and interactions of **8-PC** cation (left) and acetyl salicylate anion (right) in the active site of COX-2 enzyme.

 © 2024 The Author(s). Published by the Royal Society of Chemistry

Open Access Article. Published on 10 September 2024. Downloaded on 1/15/2026 11:51:11 AM.
This article is licensed under a Creative Commons Attribution-NonCommercial 3.0 Unported Licence.

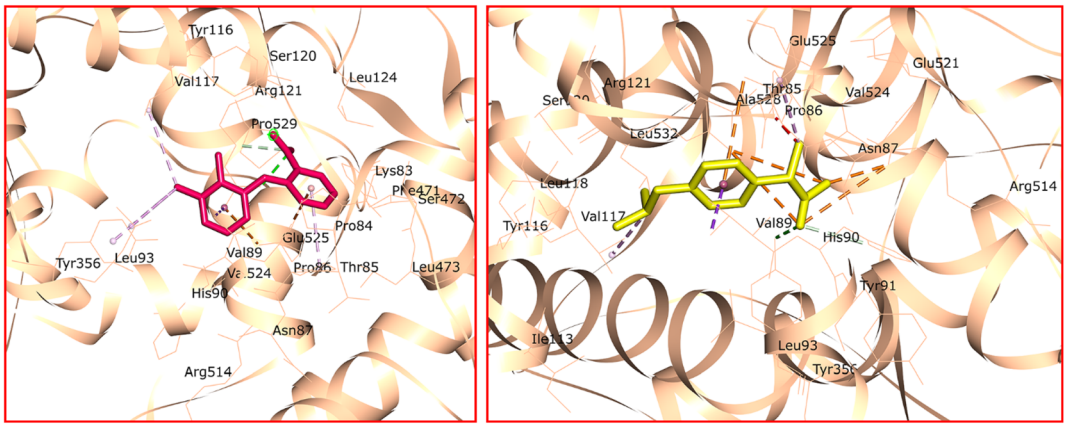

Fig. 9 Docked conformations and interactions of mefenamate (left) and ibuprofenate anions (right) in the active site of COX-2 enzyme.

noted between the phenyl rings of the mefenamate anion and Val89, Pro89, and Tyr356, respectively. Hydrophobic interactions were observed with Leu93 and Val117. Arg121 and Glu525 residues facilitated π–cation and π–anion interactions with the phenyl rings of the mefenamate anion. The mefenamate anion was surrounded by the residues Lys83, Pro84, Thr85, Pro86, His90, Leu93, Tyr116, Ser120, Leu124, Phe471, Leu473, Val524, and Ala525, participating in van der Waals interactions.

In Fig. 9 (right), a salt bridge forms between the carboxylate group of ibuprofenate and the guanidinium moiety of Arg514. The π–cation and π–anion interactions occur between the phenyl ring of the ibuprofenate anion and Arg121 and Glu525, respectively. Val89 is involved in a π–σ interaction with the ligand. Additionally, hydrophobic interactions are facilitated by Pro86 and Val117. The carboxylate group of ibuprofenate engages in a strong conventional interaction with Tyr356 and a carbon–hydrogen bond interaction with His90. An electrostatic interaction between the ibuprofenate anion and the COX-2 enzyme is observed. van der Waals interactions between the ibuprofenate anion and the COX-2 enzyme involve Pro84, Thr85, Tyr91, Thr94, Ile113, Tyr116, Leu118, Ser120, Ser354, Leu473, Glu521, Ala528, and Leu532.

The docked conformation and interactions of the naproxenate anion in the active site of the target enzyme are illustrated in Fig. 10 (left). The carboxylate group of the naproxenate anion engages in two conventional hydrogen bond interactions with Arg121 and Tyr356. Additionally, a hydrogen bond interaction was observed between Tyr116 and the methoxy group of the ligand. The naproxenate anion is further stabilized in the active site of the target enzyme through electrostatic interactions. The π–σ and π–alkyl interactions involve the residue of Val89. Moreover, additional π–alkyl interactions occur between the α-Me group of the naproxenate anion, His90, and Tyr356. Furthermore, Val89 and Leu93 contribute to hydrophobic interactions with the ligand. van der Waals interactions also play a role in stabilizing the naproxenate anion in the enzyme's active site through the residues of Lys83, Pro84, Thr85, Pro86, Tyr91, Thr94, Val117, Ser120, Leu124, Ser354, Glu521, Val524, and Ala528. Arg121 and Glu525 are involved in π–cation and π–anion interactions, respectively, with the naphthyl moiety of the naproxenate anion. The guanidinium residue of Arg514 forms a salt bridge with the carboxylate group of the ligand.

As depicted in Fig. 10 (right), Tyr365 contributed to two hydrogen bond interactions with the carboxylate and phenolic hydroxyl groups of the salicylate anion. Additionally, Arg121 engaged in a single hydrogen bond interaction with the carboxylate group of the ligand. The phenyl moiety of the

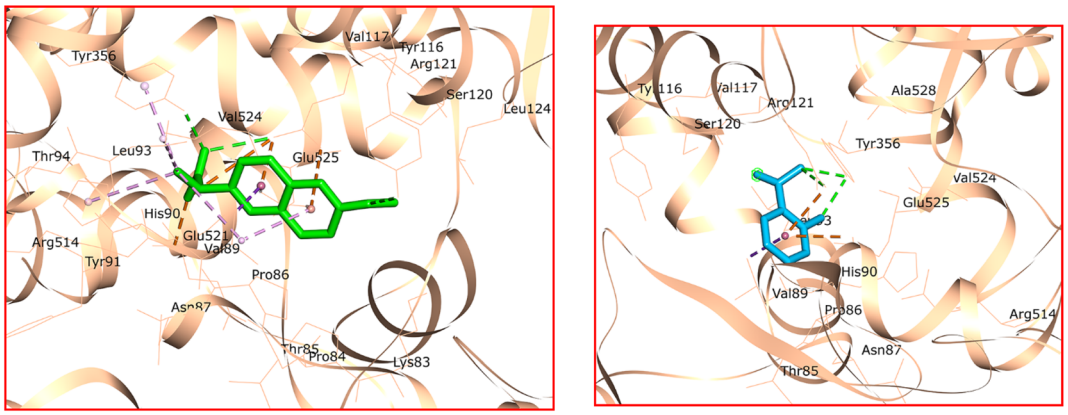

Fig. 10 Docked conformations and interactions of naproxenate (left) and salicylate anions (right) in the active site of COX-2 enzyme.

Open Access Article. Published on 10 September 2024. Downloaded on 1/15/2026 11:51:11 AM. This article is licensed under a Creative Commons Attribution-NonCommercial 3.0 Unported Licence.

salicylate anion participated in π–cation and π–anion interactions with Arg121 and Glu525, respectively, while electrostatic interactions stabilized the salicylate anion within the active site of the COX-2 enzyme. Val89 residue provided a π–sigma interaction with the phenyl ring of the salicylate anion. Furthermore, residues Pro84, Thr85, Pro86, His90, Leu93, Tyr116, Val117, Ser120, Ser354, Val524, and Ala528 contributed van der Waals interactions to stabilize the ligand in the enzyme's active site. The calculated ΔG values for IBP, **11a**, **11c**, **11d**, **11e**, and **11k** were found to be −85.67, −215.57, −239.23, −203.26, −208.12, and −226.08 kcal mol^{-1}, respectively. Analysis from molecular docking studies indicates that IBP lacks electrostatic interactions with the COX-2 enzyme's active site. However, the ILs studied herein were stabilized in the enzyme's active site through electrostatic interactions in addition to the interactions mentioned above. It is also assumed that the presence of **8-PC** cation near the active site of the COX-2 enzyme enhances the binding affinity of the tested NSAID anions, particularly ibuprofenate, compared to IBP, based on their ΔG values. Notably, the total hydrogen bond energies of the investigated ILs were at least two-fold higher than that of IBP, suggesting that hydrogen bonds and electrostatic interactions play a pivotal role in stabilizing the ligand within the COX-2 enzyme's active site and enhancing their analgesic activity.

3 Conclusion

In summary, the synthesis, analgesic, antibacterial, and docking studies of novel 8-piperazinylcaffeine carboxylate ionic liquids were studied. These salts are prepared by reacting 8-piperazinyl caffeine (**8-PC**) with various carboxylic acids, including some well-known NSAIDs. The **8-PC** salts with different NSAIDs were tested *in vivo* for analgesic properties on female mice using the formalin test. The test results showed that most of the **8-PC** and NSAID salts exhibited potent analgesic activity compared to NaIBP, a reference drug. The improved pain-relieving properties of the **8-PC**'s NSAIDs salt (**11a**, **11c–e**, and **11k**) were especially significant when compared to their sodium salt counterparts. This enhancement was linked to the inclusion of the **8-PC** cation, which contributed to a synergistic effect. Additionally, all synthesized salts were tested *in vitro* against *Staphylococcus aureus* (PTCC 1133) as a Gram-positive bacterium, *Pseudomonas aeruginosa* (ATCC 27853), and *Escherichia coli* (PTCC 1330) as Gram-negative bacteria. The results showed that salt **11k** exhibited significant antibacterial activity compared to acrinol, particularly against *P. aeruginosa* as an opportunistic and dangerous bacterium. Furthermore, docking analysis of all synthesized **8-PC** and NSAID salts (**11a**, **11c**, **11d**, **11e**, and **11k**) indicated strong binding of these salts to the active site of the COX-2 enzyme.

4 Experimental

4.1. Analgesic assessment

The formalin tests were conducted on female mice (25–30 g, $n = 21$) obtained and housed at the Comparative and Experimental Medicine Center of Shiraz University of Medical Sciences in Shiraz, Iran. The selection, care, and euthanasia of animals, as well as the experimental protocols, followed the guidelines of the Animal Care Committee of the Iran Veterinary Organization. The mice were housed in a controlled environment with a 12-hours light/dark cycle at a temperature of 25 ± 2 °C, and had unrestricted access to food and water. The animals were randomly assigned to three groups: control, positive control, and treatment (sodium ibuprofenate). Prior to the start of the experiment, the mice were acclimated to the testing environment for at least 60 minutes and placed in formalin testing chambers for a minimum of 30 minutes for habituation. A mirror was positioned underneath at a 45° angle to allow for a clear observation of the paws. The 8-piperazinylcaffeine salts of NSAIDs comprising **11a**, **11c**, **11d**, **11e**, **11k** and sodium ibuprofenate were dissolved in double distilled water and were fed orally (gavaged) to mice 10 min before pain tests. A dose of 1 μL per gram of mouse was prepared for the synthesized compounds, and each animal was then administered the dose using a specialized needle. Formalin (1%, 20 μL; subcutaneous) was injected into the right hind foot. The behaviors exhibited by the animals were observed and recorded at various time points (5, 10, 15, 20, 25, and 30 minutes) after the formalin injection. The total time (in seconds) taken for the animal to exhibit behaviors such as holding, licking, and biting the foot where formalin was injected was measured within the first 5 minutes for acute pain and up to 30 minutes for chronic pain. Any compounds labeled **11a**, **11c**, **11d**, **11e**, **11k** that can reduce this time are considered to have a more effective analgesic effect. The selection of these time intervals to assess acute and chronic pain is based on previous studies. These studies have demonstrated that the initial 5 minutes post-formalin injection, characterized by severe painful behaviors, indicate acute pain, followed by a subsequent phase of pain (chronic pain) where severe behaviors are less pronounced. The motor response to pain was recorded using a scoring system (0, 1, 2, and 3) based on the Dubuisson and Dennis method.[50,51] A score of zero indicates that the animal was in a balanced state while walking, distributing its weight evenly on both legs. A score of 1 indicates that the animal could not bear weight on the foot injected with formalin or experienced difficulty in walking. A score of 2 indicates that the animal lifted the paw with the formalin injection, keeping it off the chamber floor, and a score of 3 indicates that the animal licked or shook the formalin-injected paw. The pain score over 60 minutes was calculated in 12 blocks of 5 minutes each, with the average pain score for each block determined using a specific equation.

$$\text{Pain score} = \frac{T_0 + T_1 + T_2 + T_3}{20}$$

In this equation, T_0, T_1, T_2 and T_3 represent the counts of instances where the animal displayed zero, one, two, and three behaviors within a five-minute timeframe, each behavior lasting for 15 seconds.

4.2. Antibacterial study

The microbial concentration was adjusted to match McFarland's 0.5 turbidity standard (OD600: 0.18-0.14).[52] The minimum inhibitory concentration (MIC) values for all tested

 © 2024 The Author(s). Published by the Royal Society of Chemistry

Open Access Article. Published on 10 September 2024. Downloaded on 1/15/2026 11:51:11 AM. This article is licensed under a Creative Commons Attribution-NonCommercial 3.0 Unported Licence.

compounds were determined using a serial dilution assay and the micro-plate dilution method. The synthesized compounds were screened *in vitro* against *Staphylococcus aureus* (PTCC 1133) as a Gram-positive bacterium, *Pseudomonas aeruginosa* (ATCC 27853), and *Escherichia coli* (PTCC 1330) as Gram-negative bacteria. In a 96-well microplate, 45 microliters of culture medium, 45 microliters of synthesized compounds or ethacridine lactate (Acrinol) as a reference drug and 10 microliters of incubated bacteria were added for each microorganism. The prepared 96-well plates were then incubated for 24 hours at 37 °C. Subsequently, the optical absorbance at 600 nm was measured using an ELISA device (BioTek, Power Wave XS2). In this procedure, LB Broth with microorganisms served as the positive control, while LB Broth without microorganisms and synthesized compounds acted as the negative control. This experiment was conducted three times for validation.

4.3. Chemistry general

All chemicals were procured from Merck or other chemical suppliers and utilized without additional purification steps. The reactions were monitored using thin-layer chromatography (TLC) on SILG/UV 254 silica-gel plates. Purifications *via* short column chromatography were carried out using silica gel 60 (0.063–0.200 mm, 70–230 mesh; ASTM). Melting points were determined using the Electrothermal IA 9000 in open capillary tubes and left uncorrected. Elemental analyses, GC/MS, and IR spectra were obtained using the PerkinElmer 240-B microanalyzer, Shimadzu GC/MS-QP 1000-EX apparatus (*m*/*z*; rel.%), and Shimadzu FT-IR-8300 spectrophotometer, respectively. ^{1}H- and ^{13}C-NMR spectra were recorded on the Brüker Avance-DPX-300 spectrometer operating at 300/75 MHz, respectively. Chemical shifts are reported in δ relative to tetramethylsilane (TMS) as an internal standard, and coupling constants (*J*) are expressed in Hz. The abbreviations for ^{1}H-NMR signals include s = singlet, d = doublet, t = triplet, q = quartet, m = multiplet, br = broad, and so on.

4.3.1. Synthesis of 8-bromo-1,3,7-trimethyl-1*H*-purine-2,6(3*H*,7*H*)-dione (8-BC). Caffeine (19.4 g, 0.1 mol) and NBS (35.2 g, 0.2 mol) were added to 300 mL of freshly distilled DCM in a 500 mL round-bottom flask. After the solids dissolved, 100 mL of water was added. The mixture was shaken vigorously for 5–7 days at room temperature. Subsequently, the solution was transferred to a separator funnel, and a cold 2 M NaOH solution (100 mL) was added to decolorize it. The organic layer was separated, washed with water (2 × 200 mL), dried over Na_2SO_4 (30 g), filtered, and evaporated to yield pure **8-BC** (26 g, approximately 100% yield).[27]

4.3.2. Synthesis of 8-piperazinyl-1,3,7-trimethyl-3,7-dihydro-1*H*-purine-2,6-dione (8-PC). A mixture of anhydrous piperazine (5.2 g, 60 mmol) and **8-BC** (5.5 g, 20 mmol) in dry DMF (20 mL) was placed in a 100 mL double-necked round bottom flask with a condenser. The mixture was heated to 100 °C, and the reaction progress was monitored using TLC. After 3 hours, when TLC indicated the reaction was complete, the reaction was stopped, and the solution was cooled to room temperature. The resulting precipitates were filtered, washed with cold acetone (30 mL), and the obtained solid was either recrystallized in hot $CHCl_3$ or purified using short column chromatography on silica gel eluting with MeOH to yield white pure crystals (2.0 g, 72%).[21]

4.3.3. Synthesis of 8-piperazinylcaffeine carboxylate ionic liquids (11a–11l). In a 100 mL round-bottom flask, **8-PC** (2.78 g, 10 mmol) and the desired carboxylic acid (10 mmol) were dissolved in freshly distilled anhydrous DCM or $CHCl_3$ (30 mL). The solution was stirred at room temperature for the specified duration as shown in Fig. 4, and the progress of the reaction was monitored using TLC. Once the TLC indicated the completion of the reaction and/or no further progress, the solvent was removed using a rotary evaporator. The resulting solid was then washed with anhydrous *n*-hexane (3 × 10 mL). The pure solid obtained was dried in a vacuum oven at 60 °C for 2 hours, sealed, and stored in a desiccator at room temperature.

4.3.4. Data of the synthesized compounds

*4.3.4.1 4-(1,3,7-Trimethyl-2,6-dioxo-2,3,6,7-tetrahydro-1H-purin-8-yl)piperazin-1-ium 2-acetoxybenzoate (**11a**).* Washing the precipitate with *n*-hexane afforded the pure product as white solid (88%); m.p.: 195–197 °C, ^{1}H NMR (DMSO-d$_6$, 300 MHz): δ_{ppm} = 3.14 (s, 3H, CH_3CO), 3.19 (s, 3H, N(1)–CH_3), 3.30 (br s, 4H, 2NCH_2), 3.36 (s, 3H, N(3)–CH_3), 3.45 (br s, 4H, 2NCH_2), 3.69 (s, 3H, N(7)–CH_3), 6.67–6.71 (m, 2H, aryl), 7.20 (t, *J* = 5.1 Hz, 1H, aryl), 7.71 (d, *J* = 5.1 Hz, 1H, aryl). ^{13}C NMR (DMSO-d$_6$, 75 MHz): δ_{ppm} = 22.23, 27.67, 29.75, 32.79, 44.70, 50.05, 107.51, 123.19, 127.05, 129.80, 130.72, 135.72, 147.13, 151.49, 154.25, 155.67, 157.52, 174.61, 176.79. IR (KBr): 3485, 3075, 2981, 1730, 1713, 1690, 1614, 1565, 1460, 1373, 1038 cm^{-1}. MS (EI): *m*/*z* (%) = 459 (27.1) [M + H]$^+$. Anal. calc. for $C_{21}H_{26}N_6O_6$: C, 55.01; H, 5.72; N, 18.33; found: C, 55.19; H, 5.93; N, 18.50.

*4.3.4.2 4-(1,3,7-Trimethyl-2,6-dioxo-2,3,6,7-tetrahydro-1H-purin-8-yl)piperazin-1-ium nicotinate (**11b**).* Washing the precipitate with *n*-hexane afforded the pure product as white solid (92%); m.p.: 175–187 °C, ^{1}H NMR ($CDCl_3$, 400 MHz): δ_{ppm} = 3.33 (br s, 4H, 2NCH_2), 3.38 (s, 3H, N(1)–CH_3), 3.51 (br s, 7H, N(3)–CH_3, 2NCH_2), 3.76 (s, 3H, N(7)–CH_3), 7.36–7.39 (m, 1H, aryl), 8.32 (d, *J* = 7.6 Hz, 1H, aryl), 8.70 (d, *J* = 3.0 Hz, 1H, aryl), 9.18 (br s, 2H, NH_2), 9.25 (s, 1H, aryl). ^{13}C NMR ($CDCl_3$, 100 MHz): δ_{ppm} = 27.92, 29.86, 32.86, 44.30, 49.83, 106.34, 125.29, 132.13, 137.46, 146.14, 151.22, 153.41, 155.05, 156.15, 157.21, 178.13. IR (KBr): 3500, 3090, 2957, 1715, 1695, 1612, 1560, 1461, 1375, 1030 cm^{-1}. MS (EI): *m*/*z* (%) = 402 (23.5) [M + H]$^+$. Anal. calc. for $C_{18}H_{23}N_7O_4$: C, 53.86; H, 5.78; N, 24.43; found: C, 53.70; H, 5.89; N, 24.29.

*4.3.4.3 4-(1,3,7-Trimethyl-2,6-dioxo-2,3,6,7-tetrahydro-1H-purin-8-yl)piperazin-1-ium 2-((2,3-dimethylphenyl)amin o) benzoate (**11c**).* Washing the precipitate with *n*-hexane afforded the pure product as white solid (85%); m.p.: 195–197 °C, ^{1}H NMR (DMSO-d$_6$, 300 MHz): δ_{ppm} = 2.11 (s, 3H, PhCH_3), 2.25 (s, 3H, PhCH_3), 3.11 (br s, 4H, 2NCH_2), 3.18 (s, 3H, N(1)–CH_3), 3.34 (br s, 7H, N(3)–CH_3, 2NCH_2), 3.66 (s, 3H, N(7)–CH_3), 5.76 (s, 1H, NH), 6.59–6.64 (m, 1H, aryl), 6.79–6.88 (m, 2H, aryl), 7.01–7.06 (m, 1H, aryl), 7.12–7.18 (m, 2H, aryl), 7.89 (d, *J* = 7.5 Hz, 1H, aryl). ^{13}C NMR (DMSO-d$_6$, 75 MHz): δ_{ppm} = 13.63, 20.28, 27.34, 29.34, 32.22, 43.23, 48.09, 104.45, 112.84, 116.01, 119.63, 124.72, 125.69, 127.88, 128.86, 129.49, 131.83, 137.48, 139.67, 146.61, 147.40, 150.85, 153.88, 155.38, 177.70. IR (KBr): 3450,

Open Access Article. Published on 10 September 2024. Downloaded on 1/15/2026 11:51:11 AM. This article is licensed under a Creative Commons Attribution-NonCommercial 3.0 Unported Licence.

3052, 2964, 1713, 1694, 1615, 1567, 1473, 1370, 1035 cm^{-1}. MS (EI): *m/z* (%) = 520 (32.5) $[M + H]^+$. Anal. calc. for $C_{27}H_{33}N_7O_4$: C, 62.41; H, 6.40; N, 18.87; found: C, 62.59; H, 6.56; N, 19.01.

*4.3.4.4 4-(1,3,7-Trimethyl-2,6-dioxo-2,3,6,7-tetrahydro-1H-purin-8-yl)piperazin-1-ium 2-(4-isobutylphenyl)propan oate (**11d**).* Washing the precipitate with *n*-hexane afforded the pure product as white solid (92%); m.p.: >200 °C (dec.), ^{1}H NMR (DMSO-d_6, 300 MHz): δ_{ppm} = 0.82 (d, *J* = 6.6 Hz, 6H, $CH(CH_3)_2$), 1.30 (d, *J* = 7.2 Hz, 3H, PhCHCH_3), 1.71 (sept., *J* = 6.6 Hz, 6H, C*H*$(CH_3)_2$), 2.37 (d, *J* = 7.2 Hz, 2H, PhCH_2), 3.05 (br s, 4H, $2NCH_2$), 3.18 (s, 3H, N(1)–CH_3), 3.29 (br s, 4H, $2NCH_2$), 3.35 (s, 3H, N(3)–CH_3), 3.54 (q, *J* = 7.2 Hz, 1H, PhC*H*CH_3), 3.66 (s, 3H, N(7)–CH_3), 7.06 (d, *J* = 7.8 Hz, 2H, aryl), 7.16 (d, *J* = 7.8 Hz, 2H, aryl). ^{13}C NMR (DMSO-d_6, 75 MHz): δ_{ppm} = 19.03, 23.45, 27.60, 29.71, 30.82, 32.75, 43.61, 45.24, 46.16, 49.41, 106.20, 129.05, 129.90, 134.38, 140.59, 147.12, 151.22, 155.09, 158.07, 178.91. IR (KBr): 3456, 3075, 2946, 1715, 1698, 1616, 1564, 1453, 1370, 1041 cm^{-1}. MS (EI): *m/z* (%) = 485 (35.4) $[M + H]^+$. Anal. Calc. for $C_{25}H_{36}N_6O_4$: C, 61.96; H, 7.49; N, 17.34; found: C, 62.10; H, 7.67; N, 17.52.

*4.3.4.5 4-(1,3,7-Trimethyl-2,6-dioxo-2,3,6,7-tetrahydro-1H-purin-8-yl)piperazin-1-ium (R)-2-(6-methoxynaphthalen-2-yl) propanoate (**11e**).* Washing the precipitate with *n*-hexane afforded the pure product as white solid (88%); m.p.: 180–182 °C, ^{1}H NMR (DMSO-d_6, 300 MHz): δ_{ppm} = 1.40 (d, *J* = 7.2 Hz, 3H, CHCH_3), 2.91 (br s, 4H, $2NCH_2$), 3.17 (br s, 7H, N(1)–CH_3, $2NCH_2$), 3.33 (s, 3H, N(3)–CH_3), 3.62 (s, 3H, N(7)–CH_3), 3.69 (q, *J* = 7.2 Hz, 1H, C*H*CH_3), 3.84 (s, 3H, OCH_3), 7.09–7.13 (m, 1H, aryl), 7.25 (s, 1H, aryl), 7.39 (d, *J* = 8.4 Hz, 1H, aryl), 7.68–7.77 (m, 3H, aryl). ^{13}C NMR (DMSO-d_6, 75 MHz): δ_{ppm} = 18.67, 27.31, 29.31, 32.28, 44.26, 45.21, 49.33, 55.09, 104.30, 105.59, 118.51, 125.40, 126.53, 126.62, 128.36, 129.00, 133.07, 137.04, 146.69, 150.84, 153.80, 155.84, 156.94, 175.96. IR (KBr): 3468, 3025, 2949, 1714, 1697, 1619, 1566, 1465, 1379, 1042 cm^{-1}. MS (EI): *m/z* (%) = 509 (32.7) $[M + H]^+$. Anal. calc. for $C_{26}H_{32}N_6O_5$: C, 61.40; H, 6.34; N, 16.52; found: C, 61.49; H, 6.51; N, 16.67.

*4.3.4.6 4-(1,3,7-Trimethyl-2,6-dioxo-2,3,6,7-tetrahydro-1H-purin-8-yl)piperazin-1-ium 2-methylbenzoate (**11f**).* Washing the precipitate with *n*-hexane afforded the pure product as white solid (90%); m.p.: 180–182 °C, ^{1}H NMR (DMSO-d_6, 400 MHz): δ_{ppm} = 2.43 (s, 3H, PhCH_3), 2.72 (br s, 4H, $2NCH_2$), 3.29 (br s, 4H, $2NCH_2$), 3.37 (s, 3H, N(1)–CH_3), 3.64 (s, 3H, N(3)–CH_3), 3.81 (s, 3H, N(7)–CH_3), 7.19 (br s, 4H, aryl). ^{13}C NMR (DMSO-d_6, 100 MHz): δ_{ppm} = 18.87, 27.04, 29.02, 32.44, 43.98, 49.26, 105.81, 127.51, 128.92, 129.82, 135.26, 138.04, 140.27, 146.93, 151.02, 153.72, 157.09, 175.47. IR (KBr): 3500, 3064, 2970, 1711, 1693, 1618, 1571, 1480, 1372, 1040 cm^{-1}. MS (EI): *m/z* (%) = 415 (27.3) $[M + H]^+$. Anal. calc. for $C_{20}H_{26}N_6O_4$: C, 57.96; H, 6.32; N, 20.28; found: C, 58.19; H, 6.18; N, 20.41.

*4.3.4.7 4-(1,3,7-Trimethyl-2,6-dioxo-2,3,6,7-tetrahydro-1H-purin-8-yl)piperazin-1-ium benzoate (**11g**).* Washing the precipitate with *n*-hexane afforded the pure product as white solid (80%); m.p.: 161–163 °C, ^{1}H NMR (DMSO-d_6, 300 MHz): δ_{ppm} = 3.08 (br s, 4H, $2NCH_2$), 3.15 (s, 3H, N(1)–CH_3), 3.32 (br s, 7H, N(3)–CH_3, $2NCH_2$), 3.64 (s, 3H, N(7)–CH_3), 7.38–7.48 (m, 3H, aryl), 7.90 (d, *J* = 7.2 Hz, 2H, aryl). ^{13}C NMR (DMSO-d_6, 75 MHz): δ_{ppm} = 27.45, 29.48, 32.54, 44.34, 49.59, 107.35, 128.30, 129.38, 135.81, 138.16, 147.23, 151.62, 155.06, 157.75, 176.31. IR (KBr): 3470, 3049, 2967, 1717, 1690, 1621, 1561, 1478, 1370, 1039 cm^{-1}. MS (EI): *m/z* (%) = 401 (25.8) $[M + H]^+$. Anal. calc. for $C_{19}H_{24}N_6O_4$: C, 56.99; H, 6.04; N, 20.99; found: C, 56.78; H, 5.89; N, 20.80.

*4.3.4.8 4-(1,3,7-Trimethyl-2,6-dioxo-2,3,6,7-tetrahydro-1H-purin-8-yl)piperazin-1-ium 3-cyclohexylpropanoate (**11h**).* Washing the precipitate with *n*-hexane afforded the pure product as white solid (90%); m.p.: 102–104 °C, ^{1}H NMR ($CDCl_3$, 400 MHz): δ_{ppm} = 1.10–1.20 (m, 4H, $2CH_2$), 1.46–1.52 (m, 2H, C$H_2CH_2CO_2$), 1.61–1.68 (m, 7H, $3CH_2$, CH), 2.25 (d, *J* = 7.6 Hz, 2H, CH_2CO_2), 3.20 (br s, 4H, $2NCH_2$), 3.37 (br s, 7H, N(1)–CH_3, $2NCH_2$), 3.51 (s, 3H, N(3)–CH_3), 3.74 (s, 3H, N(7)–CH_3), 8.84 (s, 2H, NH_2). ^{13}C NMR ($CDCl_3$, 100 MHz): δ_{ppm} = 26.01, 27.92, 28.96, 29.93, 31.26, 32.80, 34.06, 34.76, 36.38, 43.89, 48.78, 107.46, 147.05, 151.96, 155.31, 157.56, 176.33. IR (KBr): 3480, 2969, 1712, 1690, 1618, 1558, 1371, 1037 cm^{-1}. MS (EI): *m/z* m (%) = 435 (28.7) $[M + H]^+$. Anal. calc. for $C_{21}H_{34}N_6O_4$: C, 58.05; H, 7.89; N, 19.34; found: C, 58.19; H, 8.06; N, 19.52.

*4.3.4.9 4-(1,3,7-Trimethyl-2,6-dioxo-2,3,6,7-tetrahydro-1H-purin-8-yl)piperazin-1-ium 4-oxopentanoate (**11i**).* Washing the precipitate with *n*-hexane afforded the pure product as white solid (85%); m.p.: 97–99 °C, ^{1}H NMR (DMSO-d_6, 400 MHz): δ_{ppm} = 2.09 (s, 3H, CH_3CO), 2.33 (t, *J* = 6.4 Hz, 2H, CH_2CO_2), 2.61 (t, *J* = 6.4 Hz, 2H, C$H_2CH_2CO_2$), 2.87 (br s, 4H, $2NCH_2$), 3.17 (br s, 7H, N(1)–CH_3, $2NCH_2$), 3.34 (s, 3H, N(3)–CH_3), 3.64 (s, 3H, N(7)–CH_3). ^{13}C NMR (DMSO-d_6, 100 MHz): δ_{ppm} = 27.62, 29.21, 30.31, 31.40, 32.91, 41.12, 43.69, 48.49, 107.40, 147.18, 151.30, 153.93, 156.01, 179.57, 189.23. IR (KBr): 3500, 2971, 1720, 1710, 1698, 1615, 1552, 1368, 1031 cm^{-1}. MS (EI): *m/z* (%) = 395 (22.6) $[M + H]^+$. Anal. calc. for $C_{17}H_{26}N_6O_5$: C, 51.77; H, 6.64; N, 21.31; found: C, 51.65; H, 6.79; N, 21.51.

*4.3.4.10 4-(1,3,7-Trimethyl-2,6-dioxo-2,3,6,7-tetrahydro-1H-purin-8-yl)piperazin-1-ium picolinate (**11j**).* Washing the precipitate with *n*-hexane afforded the pure product as white solid (80%); m.p.: 189–191 °C, ^{1}H NMR (DMSO-d_6, 300 MHz): δ_{ppm} = 3.17 (s, 3H, N(1)–CH_3), 3.29–3.34 (complex, 11H, N(3)–CH_3, $4NCH_2$), 3.67 (s, 3H, N(7)–CH_3), 6.71 (d, *J* = 9.0 Hz, 2H, aryl), 7.21–7.24 (m, 2H, aryl), 7.63 (s, 2H, NH_2). ^{13}C NMR (DMSO-d_6, 75 MHz): δ_{ppm} = 27.73, 29.71, 32.64, 43.97, 49.35, 105.61, 121.62, 128.68, 137.78, 147.78, 148.98, 151.74, 153.32, 155.45, 157.42, 175.92. IR (KBr): 3470, 3050, 2954, 1713, 1695, 1607, 1582, 1479, 1370, 1035 cm^{-1}. MS (EI): *m/z* (%) = 402 (24.9) $[M + H]^+$. Anal. calc. for $C_{18}H_{23}N_7O_4$: C, 53.86; H, 5.78; N, 24.43; found: C, 53.98; H, 5.67; N, 24.26.

*4.3.4.11 4-(1,3,7-Trimethyl-2,6-dioxo-2,3,6,7-tetrahydro-1H-purin-8-yl)piperazin-1-ium 2-hydroxybenzoate (**11k**).* Washing the precipitate with *n*-hexane afforded the pure product as white solid (92%); m.p.: 188–190 °C, ^{1}H NMR (DMSO-d_6, 300 MHz): δ_{ppm} = 3.16 (s, 3H, N(1)–CH_3), 3.33 (br s, 7H, N(3)–CH_3, $2NCH_2$), 3.45 (br s, 4H, $2NCH_2$), 3.67 (s, 3H, N(7)–CH_3), 6.64–6.70 (m, 2H, aryl), 7.18–7.23 (m, 1H, aryl), 7.69–7.27 (m, 1H, aryl), 9.82 (br s, 1H, OH). ^{13}C NMR (DMSO-d_6, 75 MHz): δ_{ppm} = 27.14, 29.03, 32.01, 43.97, 49.19, 106.39, 118.15, 122.06, 124.34, 130.58, 135.69, 146.22, 151.23, 153.52, 156.47, 158.49, 176.92. IR (KBr): 3492, 3043, 2967, 1710, 1698, 1612, 1574, 1463, 1370, 1035 cm^{-1}. MS (EI): *m/z* (%) = 417 (26.7) $[M + H]^+$. Anal. calc. for

 © 2024 The Author(s). Published by the Royal Society of Chemistry

Open Access Article. Published on 10 September 2024. Downloaded on 1/15/2026 11:51:11 AM. This article is licensed under a Creative Commons Attribution-NonCommercial 3.0 Unported Licence.

$C_{19}H_{24}N_6O_5$: C, 54.80; H, 5.81; N, 20.18; found: C, 54.92; H, 5.67; N, 20.02.

*4.3.4.12 4-(1,3,7-Trimethyl-2,6-dioxo-2,3,6,7-tetrahydro-1H-purin-8-yl)piperazin-1-ium 6-chloronicotinate (**11l**).* Washing the precipitate with *n*-hexane afforded the pure product as white solid (73%); m.p.: 149–151 °C, ^{1}H NMR (DMSO-d$_6$, 300 MHz): δ_{ppm} = 3.16 (s, 3H, N(1)–CH$_3$), 3.27 (br s, 4H, 2NCH$_2$), 3.33 (s, 3H, N(3)–CH$_3$), 3.44 (br s, 4H, 2NCH$_2$), 3.66 (s, 3H, N(7)–CH$_3$), 7.52 (d, J = 8.1 Hz, 1H, aryl), 8.20 (d, J = 7.8 Hz, 1H, aryl), 8.82 (s, 1H, aryl). ^{13}C NMR (DMSO-d$_6$, 75 MHz): δ_{ppm} = 27.21, 29.68, 32.09, 43.79, 48.76, 105.07, 125.30, 130.34, 140.18, 147.09, 150.83, 153.81, 154.85, 155.62, 157.68, 178.03. IR (KBr): 3475, 3073, 2961, 1710, 1696, 1612, 1578, 1446, 1370, 1032, 1019 cm^{-1}. MS (EI): m/z (%) = 436 (21.8) [M + H]$^+$. Anal. calc. for $C_{18}H_{22}ClN_7O_4$: C, 49.60; H, 5.09; N, 22.49; found: C, 49.45; H, 5.22; N, 22.30.

Data availability

Data will be made available on request.

Conflicts of interest

The authors declare that they have no known competing financial interests or personal relationships that could have appeared to influence the work reported in this paper.

Acknowledgements

The authors wish to thank Shiraz University of Technology research council for partial support of this work.

References

1 N. Abidi and J. L. Shamshina, *Properties and Applications of Ionic Liquids*, Nova Science Publishers, Inc., 1st edn, 2023.
2 J. L. Shamshina and R. D. Rogers, Ionic liquids: new forms of active pharmaceutical ingredients with unique, tunable properties, *Chem. Rev.*, 2023, **123**, 11894–11953.
3 R. Ferraz, L. C. Branco, C. Prudêncio, J. P. Noronha and Z. Petrovski, Ionic liquids as active pharmaceutical ingredients, *ChemMedChem*, 2011, **6**, 975–985.
4 P. Walden, Molecular weights and electrical conductivity of several fused salts, *Bull. Acad. Sci. St. Petersbourg*, 1914, 405–422.
5 M. Deetlefs, K. R. Seddon and M. Shara, Predicting physical properties of ionic liquids, *Phys. Chem. Chem. Phys.*, 2006, **8**, 642–649.
6 D. M. Correia, L. C. Fernandes, M. M. Fernandes, B. Hermenegildo, R. M. Meira, C. Ribeiro, S. Ribeiro, J. Reguera and S. Lanceros-Méndez, Ionic Liquid-Based Materials for Biomedical Applications, *Nanomater.*, 2021, **11**, 2401.
7 W. L. Hough, M. Smiglak, H. Rodríguez, R. P. Swatloski, S. K. Spear, D. T. Daly, J. Pernak, J. E. Grisel, R. D. Carliss, M. D. Soutullo, J. H. Davis, Jr and R. D. Rogers, The third evolution of ionic liquids: active pharmaceutical ingredients, *New J. Chem.*, 2007, **31**, 1429–1436.
8 V. Kumar and S. V. Malhotr, *Ionic Liquids as Pharmaceutical Salts: A Historical Perspective*, ACS Symposium Series, American Chemical Society, Washington, DC, 2010, ch. 1.
9 S. N. Pedro, C. S. R. Freire, A. J. D. Silvestre and M. G. Freire, The Role of ionic liquids in the pharmaceutical field: an overview of relevant applications, *Int. J. Mol. Sci.*, 2020, **21**, 8298.
10 M. Handa, W. H. Almalki, R. Shukla, O. Afzal, A. S. A. Altamimi, S. Beg and M. Rahman, Active pharmaceutical ingredients (APIs) in ionic liquids: An effective approach for API physiochemical parameter optimization, *Drug Discovery Today*, 2022, **27**, 2415–2424.
11 S. N. Pedro, C. S. R. Freire, A. J. D. Silvestre and M. G. Freire, The role of ionic liquids in the pharmaceutical field: an overview of relevant applications, *Int. J. Mol. Sci.*, 2020, **21**, 8298.
12 N. Singh, A. K. Shreshtha, M. S. Thakur and S. Patra, Xanthine scaffold: scope and potential in drug development, *Heliyon*, 2018, **4**, e00829.
13 A. Kapri, N. Gupta and S. Nain, Recent advances in the synthesis of xanthines: a short review, *Scientifica*, 2022, **2022**, 1–24.
14 M. N. Soltani Rad, S. Behrouz, S. Aghajani, M. Behrouz, E. Zarenezhad and A. Ghanbariasad, Design, synthesis, anticancer and in silico assessment of 8-caffeinyl-triazolylmethoxy hybrid conjugate, *RSC Adv.*, 2023, **13**, 3056–3070.
15 R.-H. Zhang, H.-Y. Guo, H. Deng, J. Lia and Z.-S. Quan, Piperazine skeleton in the structural modification of natural products: a review, *J. Enzyme Inhib. Med. Chem.*, 2021, **36**, 1165–1197.
16 M. Shaquiquzzaman, G. Verma, A. Marella, M. Akhter, W. Akhtar, M. F. Khan, S. Tasneem and M. Mumtaz Alam, Piperazine scaffold: A remarkable tool in generation of diverse pharmacological agents, *Eur. J. Med. Chem.*, 2015, **102**, 487–529.
17 S. Serin, DFT-based computations on some structurally related N-substituted piperazines, *J. Indian Chem. Soc.*, 2022, **99**, 100766.
18 A. Kleeman, J. Engel, B. Kutscher and D. Reichert, *Pharmaceutical Substances*, Thieme, Stuttgart, 3rd edn, 1999.
19 M. N. Romanelli, L. Braconi, A. Gabellini, D. Manetti, G. Marotta and E. Teodori, Synthetic approaches to piperazine-containing drugs approved by FDA in the period of 2011–2023, *Molecules*, 2024, **29**, 68.
20 F. Himmelsbach, E. Langkopf, M. Eckhardt, M. Tadayyon and L. Tomas, Novel 8-(Piperazine-1-yl)- and 8-(1,4 Diazepan-1-yl)-xanthine, the production and use thereof in the form of a drug, *Eur. Patent*, 1689748B1, 2008.
21 M. N. Soltani Rad, S. Behrouz, K. Zokaei, M. Behrouz, A. Ghanbariasad and E. Zarenezhad, Synthesis of some novel 8-(4-alkylpiperazinyl) caffeine derivatives as potent anti-leishmania agents, *Bioorg. Chem.*, 2022, **128**, 106062.
22 M. N. Soltani Rad, S. Behrouz, K. Shahbazkhani, M. Behrouz, E. Zarenezhad and A. Ghanbariasad, Design, synthesis,

Open Access Article. Published on 10 September 2024. Downloaded on 1/15/2026 11:51:11 AM.
This article is licensed under a Creative Commons Attribution-NonCommercial 3.0 Unported Licence.

anticancer and in silico assessment of 8-piperazinyl caffeinyl-triazolylmethyl hybrid conjugates, *RSC Adv.*, 2023, **13**, 24656–24673.

23 S. N. Raja, D. B. Carr, M. Cohen, N. B. Finnerup, H. Flor, S. Gibson, F. Keefe, J. S. Mogil, M. Ringkamp, K. A. Sluka, X.-J. Song, B. Stevens, M. Sullivan, P. Tutelman, T. Ushida and K. Vader, The revised IASP definition of pain: concepts, challenges, and compromises, *Pain*, 2020, **161**, 1976–1982.

24 C. Patrono and B. Rocca, Nonsteroidal antiinflammatory drugs: past, present and future, *Pharmacol. Res.*, 2009, **59**, 285–289.

25 S. Bindu, S. Mazumder and U. Bandyopadhyay, Non-steroidal anti-inflammatory drugs (NSAIDs) and organ damage: A current perspective, *Biochem. Pharmacol.*, 2020, **180**, 114–147.

26 V. C. Ziesenitz, T. Welzel, M. van Dyk, P. Saur, M. Gorenflo and J. N. van den Anker, Efficacy and safety of NSAIDs in infants: a comprehensive review of the literature of the past 20 years, *Paediatr. Drugs*, 2022, **24**, 603–655.

27 M. N. Soltani Rad and S. Maghsoudi, Two-step three-component process for one-pot synthesis of 8-alkylmercaptocaffeine derivatives, *RSC Adv.*, 2016, **6**, 70335–70342.

28 J. Mitkov, M. Georgieva and A. Zlatkov, Development of an optimized synthetic approach for synthesis of caffeine-8-thioglycolic acid and its ester derivatives, *Pharmacy*, 2012, **1–4**, 17–23.

29 J. Mitkov, L. Nikolova, I. Nikolova, N. Danchev and A. Zlatkov, Synthesis and brain antihypoxic activity of some aminoalcoholic derivatives of caffeine-8-thioglycolic acid, *C. R. Acad. Bulg. Sci.*, 2010, **63**, 1075–1082.

30 D. J. Langford and J. S. Mogil, *Anesthesia and Analgesia in Laboratory Animals*, Elsevier Science, 2008.

31 N. Veronese, F. Ecarnot, S. Cheleschi, A. Fioravanti and S. Maggi, Possible synergic action of non-steroidal anti-inflammatory drugs and glucosamine sulfate for the treatment of knee osteoarthritis: a scoping review, *BMC Musculoskeletal Disord.*, 2022, **23**, 1084.

32 M. I. Ortiz, M. P. González-García, H. A. Ponce-Monter, G. Castañeda-Hernández and P. Aguilar-Robles, Synergistic effect of the interaction between naproxen and citral on inflammation in rats, *Phytomedicine*, 2010, **18**, 74–79.

33 M. A. De Paz-Campos, M. I. Ortiz, A. E. Chávez Piña, L. Zazueta-Beltrán and G. Castañeda-Hernández, Synergistic effect of the interaction between curcumin and diclofenac on the formalin test in rats, *Phytomed*, 2014, **21**, 1543–1548.

34 D. Ialongo, V. Tudino, M. Arpacioglu, A. Messore, E. Patacchini, R. Costi, R. Di Santo and V. N. Madia, Synergistic effects of caffeine in combination with conventional drugs: Perspectives of a drug that never ages, *Pharmaceuticals*, 2023, **16**, 730.

35 V. A. Voicu, C. Mircioiu, C. Plesa, M. Jinga, V. Balaban, R. Sandulovici, A. M. Costache, V. Anuta and I. Mircioiu, Effect of a new synergistic combination of low doses of acetylsalicylic acid, caffeine, acetaminophen, and chlorpheniramine in acute low back pain, *Front. Pharmacol.*, 2019, **10**, 1–15.

36 A. Borówka, A. Sierosławska, A. Baier, A. Rymuszka and E. Olszewska, Silver and copper complexes with ibuprofen and caffeine-preparation and evaluation of their selected biological effects, *Molecules*, 2024, **29**, 506.

37 A. Straube, B. Aicher, B. L. Fiebich and G. Haag, Combined analgesics in (headache) pain therapy: shotgun approach or precise multi-target therapeutics?, *BMC Neurol.*, 2011, **11**, 43.

38 J. R. M. López, A. M. Domínguez-Ramírez, H. J. Cook, G. Bravo, Ma. I. Díaz-Reval, M. Déciga-Campos and F. J. López-Muñoz, Enhancement of antinociception by co-administration of ibuprofen and caffeine in arthritic rats, *Eur. J. Pharmacol.*, 2006, **544**, 31–38.

39 P. Barbanti, G. Allais, S. Cevoli, S. Guerzoni, M. Valeriani and F. Vernieri, The role of the combination paracetamol/caffeine in treatment of acute migraine pain: a narrative review, *Pain Ther.*, 2024, **13**, 319–346.

40 N. Ahmadi, H. Salimizand, A. R. Zomorodi, J. E. Abbas, R. Ramazanzadeh, F. Haghi, S. Hassanzadeh, M. Jahantigh and M. Shahin, Genomic diversity of β-lactamase producing Pseudomonas aeruginosa in Iran; the impact of global high-risk clones, *Ann. Clin. Microbiol. Antimicrob.*, 2024, **23**, 5.

41 X. Song, R. Li, Q. Zhang, S. He and Y. Wang, Antibacterial effect and possible mechanism of salicylic acid microcapsules against escherichia coli and staphylococcus aureus, *Int. J. Environ. Res. Public Health*, 2022, **19**, 12761.

42 E. M. E. Sykes, D. White, S. McLaughlin and A. Kumar, Salicylic acids and pathogenic bacteria: new perspectives on an old compound, *Can. J. Microbiol.*, 2024, **70**, 1–14.

43 *Molegro Virtual Docker, Version 6.0.0, CLC Bio, 8200, Aarhus, N.; Denmark*, 2012.

44 O. Laneuville, D. K. Breuer, D. L. Dewitt, T. Hla, C. D. Funk and W. L. Smith, Differential inhibition of human prostaglandin endoperoxide H synthases-1 and -2 by nonsteroidal anti-inflammatory drugs, *J. Pharmacol. Exp. Ther.*, 1994, **271**, 927–934.

45 M. J. Frisch, G. W. Trucks, H. B. Schlegel, G. E. Scuseria, M. A. Robb, J. R. Cheeseman, *et al.*, *Gaussian 09, Revision D.01*, Gaussian, Inc., Wallingford CT, 2013.

46 J. J. P. Stewart, Application of the PM6 method to modeling the solid state, *J. Mol. Model.*, 2008, **14**, 499–535.

47 G. Marcou and D. Rognan, Optimizing fragment and scaffold docking by use of molecular interaction fingerprints, *J. Chem. Inf. Model.*, 2007, **47**, 195–207.

48 B. J. Orlando, M. J. Lucido and M. G. Malkowski, The structure of ibuprofen bound to cyclooxygenase-2, *J. Struct. Biol.*, 2015, **189**, 62–66.

49 K. K. Angajala, S. V. Ramesh Macha, M. Raghavender, M. K. Thupurani and P. J. Pathi, Synthesis, anti-inflammatory, bactericidal activities and docking studies of novel 1,2,3-triazoles derived from ibuprofen using click chemistry, *SpringerPlus*, 2016, **5**, 423.

50 D. Dubuisson and S. G. Dennis, The formalin test: A quantitative study of the analgesic effects of morphine,

 © 2024 The Author(s). Published by the Royal Society of Chemistry

Open Access Article. Published on 10 September 2024. Downloaded on 1/15/2026 11:51:11 AM.
This article is licensed under a Creative Commons Attribution-NonCommercial 3.0 Unported Licence.

meperidin, and brain stem stimulation in rats and cats, *Pain*, 1977, **4**, 161–174.

51 A. Tjolsen, O. G. Berge, S. Hunskaar, J. H. Rosland and K. Hole, The formalin test: An evaluation of the method, *Pain*, 1992, **51**, 5–17.

52 F. R. Cockerill, M. A. Wikler, J. Alder, M. N. Dudley, G. M. Eliopoulos, M. J. Ferraro, D. J. Hardy, D. W. Hecht, J. A. Hindler, J. B. Patel, M. Powell, J. M. Swenson, R. B. Thomson, Jr, M. M. Traczewski, J. D. Turnidge, M. P. Weinstein and B. L. Zimmer, *Methods for Dilution Antimicrobial Susceptibility Tests for Bacteria that Grow Aerobically; Approved Standard*, CLSI document M07-A9, ISBN 1-56238-784-7, Clinical and Laboratory Standards Institute, 950 West Valley Road, Suite 2500, Wayne, Pennsylvania 19087, USA, 9th edn, 2012.